Impact of Communication Delays on Secondary Frequency Control in an Islanded Microgrid

Shichao Liu, Xiaoyu Wang, *Senior Member, IEEE*, and Peter Xiaoping Liu, *Senior Member, IEEE*

***Abstract*—Low-bandwidth communication channels are used to support the information exchange between a microgrid centralized controller and local controllers in the secondary frequency control of an islanded microgrid. However, the impact of the inherent time delay in these communication channels on the microgrid performance has not been taken into account when the secondary frequency controller is designed. This paper investigates the effect of the communication delays on the secondary frequency control of an islanded microgrid with multiple distributed generators. A small-signal model-based method is introduced for the microgrid to find delay margins below which the microgrid can remain stable. By performing a series of trial studies, the relationships between secondary frequency control gains and delay margins are obtained. A gain scheduling approach is also proposed to compensate the effect of the communication delay on the secondary frequency control. Results from the Canadian urban distribution system have verified that communication delays can adversely affect the microgrid secondary frequency control, and the proposed gain scheduling approach can improve the robustness of the microgrid secondary frequency controller to communication delays.**

***Index Terms*—Communication delays, gain scheduling, microgrid, secondary frequency control, small-signal model.**

I. Introduction

THE increasing penetration of distributed generation (DG) units and distributed storage (DS) units into a power grid makes the operation and control of a power distribution system quite challenging. Being an integrated energy system that comprises interconnected loads, i.e., DG and DS units, a microgrid is introduced to better organize the distribution system [1]–[4]. The two operation modes of the microgrid include the grid-connected mode and the islanded mode. In the grid-connected mode, the microgrid adjusts real and reactive power profiles by injecting a certain amount of real and reactive power into the main grid or absorbing from it. In the islanded mode, due to the lack of the main grid as a reference, the microgrid has to maintain its stable operation by coordinating all the elements of its own. The islanded operation, which is the focus of this paper, may result from either preplanned maintenance operations or unplanned switch incidents [5].

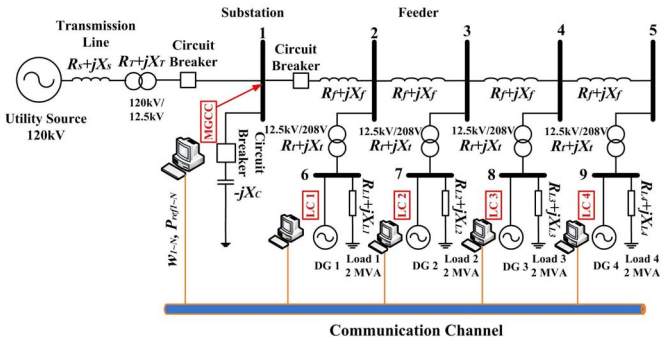

Fig. 1. Canadian urban benchmark distribution system.

The microgrid control with inverter-based DGs mainly refers to the inverter control due to the fact that it is commonly interfaced with the prime mover of each DG via a power-electronic inverter. For a microgrid with several inverters connecting with each other in parallel, droop controllers are conventionally used to regulate the real and reactive power of each inverter, including real-power/frequency droop controllers and reactive power/voltage droop controllers [6], [7]. While the droop control can achieve good real and reactive power regulation performance, it has several drawbacks such as incapability of sharing nonlinear loads, sensitivity to output and line impedances, and incapability of removing frequency deviations without frequency recovery loops [8], [9].

To restore its frequency to the nominal value in an islanded microgrid, a hierarchical inverter control structure has been proposed [10]–[15]. It includes a secondary controller in a microgrid centralized controller (MGCC) at the low-voltage side of a substation and local primary inverter controllers (LCs) for all the DGs and DSs in a microgrid. For example, Fig. 1 shows the studied Canadian urban benchmark distribution system proposed in [16] and this paper. In the primary frequency control, the LCs act fast to stabilize the frequency dynamics in case of load changes and disturbances because of their negligible inertias. In the frequency restoration, the secondary controller in MGCC generates supplementary real-power set points for the LCs and sends them through low-bandwidth communication channels.

Manuscript received April 24, 2014; revised July 29, 2014 and September 18, 2014; accepted October 10, 2014. Date of publication November 5, 2014; date of current version March 6, 2015. This work was supported in part by the Natural Sciences and Engineering Research Council of Canada and in part by the Carleton President 2010 Ph.D. Fellowship.

S. Liu and P. X. Liu are with the Department of Systems and Computer Engineering, Carleton University, Ottawa, ON K1S 5B6, Canada (e-mail: lshchao@sce.carleton.ca; xpliu@sce.carleton.ca).

X. Wang is with the Department of Electronics, Carleton University, Ottawa, ON K1S 5B6, Canada (e-mail: xiaoyuw@doe.carleton.ca).

Color versions of one or more of the figures in this paper are available online at http://ieeexplore.ieee.org.

Digital Object Identifier 10.1109/TIE.2014.2367456

While this hierarchical controller can eliminate frequency deviations of the droop controllers, it involves communications between MGCC and LCs. Until now, most researches on the hierarchical inverter control in literature have assumed that communication delays between the secondary controller and LCs are negligible. However, as a variety of open communication infrastructures including Ethernet, Internet, WiMax, and WiFi are increasingly implemented for smart grid communications, power control and measurement signals may be delayed or dropped during their transmission [17]–[21]. In terms of network-induced time delays, their characteristics can be constant, bounded, or random, depending on the inner mechanisms of the communication systems adopted [22]. Aside from time delays, sampling rates in these communication systems might also affect the microgrid performance. However, sampling rates of these communication systems are very fast, such as Ethernet (Megabits date rats), Wireless Ethernet (Gigabit date rates), and Power Line Communication (9600 to 19200 b/s). In contrast, the data volume of the secondary control signals in the studied microgrid is less than 100 bytes [23]. Thus, the communication delay is the focus of this paper. In fact, time delays are inherent in these communication infrastructures. This indicates that it is critical to take the impact of communication delays into account when the hierarchical inverter control is designed for microgrids.

The objective of this paper is to study the hierarchical inverter control by taking into account the communication delay effect in islanded microgrids. We mainly focus on the microgrid with inverter-based DGs such as photovoltaics (PVs) and fuel cells [24]–[26]. These inverter-based DGs can act very fast to load changes and disturbances because of their negligible inertias. After receiving the supplementary set points generated by the secondary controller in the MGCC, these DGs can take action in a short time. Therefore, we believe communication delays could adversely affect this type of microgrid. To verify this point, the impact of communication delay on the performance of an islanded microgrid is investigated. A small-signal model-based method is introduced to determine the communication delay margin below which the microgrid system can stay stable. By conducting a series of trial studies, we find the relationships between delay margins and secondary frequency control gains. To compensate the communication delay effect on the system performance, a new gain-scheduling frequency control approach is also proposed for the islanded microgrid. Studies of the Canadian urban benchmark distribution system have validated the impact of communication delays on the microgrid performance and the effectiveness of the proposed gain-scheduling frequency control approach.

The remainder of this paper is organized as follows. The effect of communication delays on the microgrid is investigated in Section II. A gain-scheduling approach is proposed to compensate the communication delay effect in Section III. Results of the Canadian urban distribution system are shown to validate the proposed analysis and gain-scheduling approach in Section IV. In Section V, more discussions on the hierarchical frequency control are made. Finally, Conclusions and future work are summarized in Section VI.

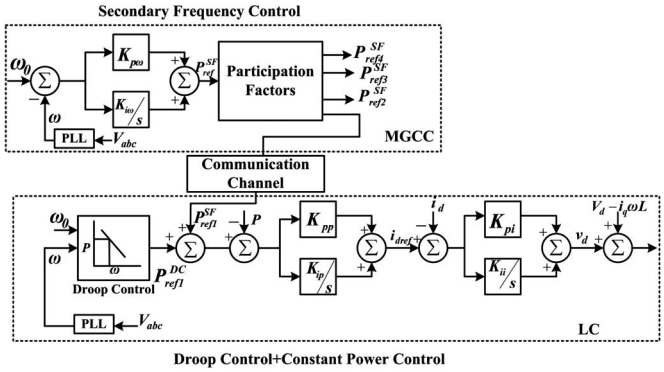

Fig. 2. Structure of the multi-DG system two-level control.

II. Analysis of the Time-Delay Effect on the Islanded Microgrid Performance

A. Small-Signal Model of the Islanded Microgrid With Communication Delays

The Canadian urban benchmark distribution system shown in Fig. 1 is used to investigate the secondary frequency control of microgrids here. It has been used in several microgrid studies [16], [27], [28]. The detailed parameters of the system is shown in Tables I and II in Appendix B. The utility source is 120 kV, and the 12.5-kV substation is connected to the grid through a circuit breaker (CB) and a substation transformer with a capacity of 10 MVA. A 2.75-Mvar capacitor bank is located at the substation. Four inverter-based DGs (three-phase 208 V) are evenly distributed along the feeder. They are connected to the feeder through the step-down transformers and the DG terminals are from Node 6 to Node 9 in sequence. The constant impedance load model with power factor 0.95 is adopted to represent the local load of each generator. Since our focus is the communication delay effect on the microgrid dynamics, the measurement filter of active power in the inverter side has not been included.

The small-signal model of this microgrid consists of three blocks, including the DG block, the network block, and the load block, as well as the interface block. The model of the inverter-based DG with the secondary controller is described as follows.

The hierarchical control structure of the microgrid is shown in Fig. 2. The power control loop of the local primary controller of a DG inverter consists of a power control and an inner current loop, to regulate the inverter output power by tracking given real-power set points. Both the power and current controllers are proportional–integral (PI) controllers. The power controller is

$$i_{\mathrm{dref}i} = \left(K_{ppi} + \frac{K_{ipi}}{s}\right)\left(P_{\mathrm{ref}i}^{\mathrm{SF}} + P_{\mathrm{ref}i}^{\mathrm{DC}} - P_i\right) \tag{1}$$

$$i_{\mathrm{qref}i} = \left(K_{ppi} + \frac{K_{ipi}}{s}\right)\left(Q_{\mathrm{ref}i} - Q_i\right) \tag{2}$$

where $i_{\mathrm{dref}i}$ and $i_{\mathrm{qref}i}$ are the components of the current set points on d-axis (direct) and q-axis (quadrature) of the ith DG, and K_{ppi} and K_{ipi} are the proportional and integral control gains of the ith DG, respectively; $P_{\mathrm{ref}i}^{\mathrm{SF}}$ is the ith DG supplementary real-power set point assigned by the secondary

frequency controller of MGCC; $P_{\mathrm{ref}i}^{\mathrm{DC}}$ is the corrective real-power set point generated by the power control of ith DG; and P_i and Q_i are the instantaneous real and reactive power. $Q_{\mathrm{ref}i}$ is the reactive power set point of ith DG. Since the focus of this paper is the frequency control, only a real-power control structure is shown in Fig. 2

$$v_{di} = \left(K_{pii} + \frac{K_{iii}}{s}\right)(i_{\mathrm{dref}i} - i_{di}) \tag{3}$$

$$v_{qi} = \left(K_{pii} + \frac{K_{iii}}{s}\right)(i_{\mathrm{qref}i} - i_{qi}) \tag{4}$$

where v_{di} and v_{qi} are the components of the voltage set points on d- and q-axis of the ith DG, i_{di} and i_{qi} are the instantaneous currents of the ith DG.

The $\omega - P$ characteristic of the frequency droop control can be described as

$$P_{\mathrm{ref}i}^{\mathrm{DC}} = K_{\omega i}(\omega_0 - \omega_i) \tag{5}$$

where K_ω is the droop control gain, $P_{\mathrm{ref}i}^{\mathrm{DC}}$ is the corrective power set point due to frequency variations. The secondary frequency control is

$$P_{\mathrm{ref}i}^{\mathrm{SF}} = \left(K_{p\omega i} + \frac{K_{i\omega i}}{s}\right)(\omega_0 - \omega_i) \tag{6}$$

where $P_{\mathrm{ref}i}^{\mathrm{SF}}$ is the supplementary power set point of the ith DG assigned by the secondary frequency controller, $K_{p\omega i}$ and $K_{i\omega i}$ are proportional and integral control gains, respectively; ω_0 is the nominal frequency reference; and ω_i is the instantaneous frequency obtained from a phase-locked loop (PLL). As shown in Fig. 2, a PLL is also installed at the MGCC to measure the microgrid frequency.

The PLL model can be expressed as

$$\omega_{\mathrm{PLL}i} = \left(K_{p\mathrm{PLL}i} + \frac{K_{i\mathrm{PLL}i}}{s}\right)V_{qi} - \omega_0 \tag{7}$$

where $\omega_{\mathrm{PLL}i}$ is the tracked voltage frequency, V_{qi} is the q-axis voltage obtained by using the $abc{-}dq$ transformation, ω_0 is the nominal frequency, and $K_{p\mathrm{PLL}i}$ and $K_{i\mathrm{PLL}i}$ are the PI controller gains of the ith DG.

The second part of the microgrid model is the network block, which can be written in a common reference frame as follows:

$$\begin{bmatrix}\Delta\mathbf{i_x}\\ \Delta\mathbf{i_y}\end{bmatrix} = \begin{bmatrix}\mathbf{G} & -\mathbf{B}\\ \mathbf{B} & \mathbf{G}\end{bmatrix}\begin{bmatrix}\Delta\mathbf{V_x}\\ \Delta\mathbf{V_y}\end{bmatrix} \tag{8}$$

where the matrices $\mathbf{G}$ and $\mathbf{B}$ are acquired from the network system admittance matrix and $\mathbf{V_x} = [V_{x1}, V_{x2}, \ldots, V_{xn}]^T$, $\mathbf{V_y} = [V_{y1}, V_{y2}, \ldots, V_{yn}]^T$, and $\mathbf{i_x} = [i_{x1}, i_{x2}, \ldots, i_{xn}]^T$, $\mathbf{i_y} = [i_{y1}, i_{y2}, \ldots, i_{yn}]^T$.

The third part of the microgrid small-signal model is the interface block. Among mathematic equations obtained above, each DG model is developed in its own $d{-}q$ reference frame. To develop the small-signal model of the microgrid, all the voltages and currents must be transformed to the common reference $x{-}y$ frame. The reference frame transformation between local

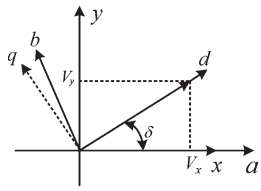

Fig. 3. Reference frame transformation.

$d{-}q$ reference frame and the common $x{-}y$ reference frame is shown in Fig. 3. The interface equations are

$$\Delta\mathbf{V_d} = \mathbf{C_0}\Delta\mathbf{V_x} - \mathbf{V_{x0}}\mathbf{S_0}\Delta\delta + \mathbf{S_0}\Delta\mathbf{V_y} + \mathbf{V_{y0}}\mathbf{C_0}\Delta\delta \tag{9}$$

$$\Delta\mathbf{V_q} = \mathbf{S_0}\Delta\mathbf{V_x} - \mathbf{V_{x0}}\mathbf{C_0}\Delta\delta + \mathbf{C_0}\Delta\mathbf{V_y} + \mathbf{V_{y0}}\mathbf{S_0}\Delta\delta \tag{10}$$

$$\Delta\mathbf{i_x} = \mathbf{C_0}\Delta\mathbf{i_d} - \mathbf{i_{d0}}\mathbf{S_0}\Delta\delta - \mathbf{S_0}\Delta\mathbf{i_q} - \mathbf{i_{q0}}\mathbf{C_0}\Delta\delta \tag{11}$$

$$\Delta\mathbf{i_y} = \mathbf{S_0}\Delta\mathbf{i_d} + \mathbf{i_{d0}}\mathbf{C_0}\Delta\delta + \mathbf{C_0}\Delta\mathbf{i_q} - \mathbf{i_{q0}}\mathbf{S_0}\Delta\delta \tag{12}$$

where δ_i is the individual inverter terminal voltage phase angle in the $x{-}y$ reference frame, and the diagonal matrices $\mathbf{C_0}$ and $\mathbf{S_0}$ are defined as $\mathbf{C_0} = \mathrm{diag}\{\cos(\delta_{i0})\}$ and $\mathbf{S_0} = \mathrm{diag}\{\sin(\delta_{i0})\}$, respectively.

Based on the aforementioned discussion and our previous work [16], the state space of the overall system is formulated as the following descriptor system:

$$\mathbf{E}\Delta\dot{\mathbf{x}} = \mathbf{A}\Delta\mathbf{x} + \mathbf{F}\mathbf{r_0} \tag{13}$$

where $\mathbf{x} = [\boldsymbol{\delta}, \boldsymbol{\omega}, \mathbf{i_d}, \mathbf{i_q}, \mathbf{i_{dref}}, \mathbf{i_{qref}}, \mathbf{u_d}, \mathbf{u_q}, \mathbf{P}, \mathbf{Q}, \mathbf{P_{ref}}, \mathbf{V_d}, \mathbf{V_q}, \mathbf{i_x}, \mathbf{i_y}, \mathbf{V_x}, \mathbf{V_y}]^T$, $\mathbf{r}, \mathbf{0} = [\boldsymbol{\omega_0}]^T$, $\mathbf{E}$ is a system matrix, which is singular, $\mathbf{A}$ is the system matrix, and $\mathbf{F}$ is a parameter matrix.

By leaving all the derivatives of the state variables on the left sides of the physical equations and moving other parts to the right sides of these equations, (13) can be derived. In the descriptor system, matrix E is squared and can be singular, which is not necessarily an identical matrix as in the case of regular systems. Components of E and A are shown in Appendix A.

Consider a time delay τ exists in communication channels between MGCC and LCs. The overall system model becomes a time-delay descriptor system, which is written as

$$\mathbf{E}\Delta\dot{\mathbf{x}} = \mathbf{A}\Delta\mathbf{x} + \mathbf{A}_\tau\Delta\mathbf{x}(\mathbf{t} - \tau) + \mathbf{F}\mathbf{r_0} \tag{14}$$

where τ denotes a time delay, $\mathbf{x}(\mathbf{t} - \boldsymbol{\tau})$ is the time-delayed state, and $\mathbf{A}_\tau$ is its parameter matrix.

B. Effects of Time Delays on the Microgrid Performance

The characteristic equation of the delayed descriptor system (14) is

$$\det\left(\lambda\mathbf{E} - \Delta(\lambda, \tau)\right) = 0 \tag{15}$$

where

$$\Delta(\lambda, \tau) = \mathbf{A} + \mathbf{A}_\tau e^{-\lambda\tau}. \tag{16}$$

Definition 1. [29], [30]: For a given τ, the delayed descriptor system (14) is asymptotically stable if all generalized roots of its characteristic (15) are in the open left-hand plane.

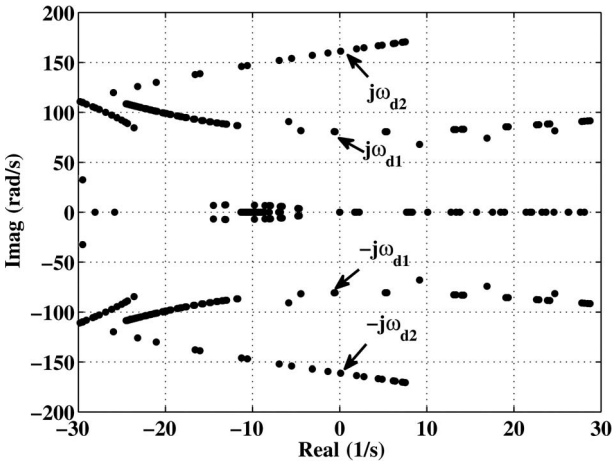

Fig. 4. Root loci of $\Delta(\eta)$ when the secondary frequency control gains are $K_{p\omega} = 2$ and $K_{i\omega} = 60$.

Definition 2: A critical delay denoted by τ_d is called a delay margin if the delayed descriptor system (9) is stable for $\tau < \tau_d$, and it is unstable for $\tau > \tau_d$.

Approaches to determine delay margins for power systems have been discussed in [31] and [32]. In this paper, an eigenvalue approach in [32] is extended to the delayed descriptor system (9).

Given a pair of generalized conjugate eigenvalues on the imaginary axis, they are denoted by $\lambda_{\text{imag}} = \pm j\omega$. The following equation is satisfied:

$$j\omega = \text{eig}\left(\Delta(\omega, \tau)\right) \tag{17}$$

where $\text{eig}(\star)$ denotes eigenvalues of $\star$, and

$$\Delta(\omega, \tau) = \mathbf{A} + \mathbf{A}_\tau e^{-j\omega\tau}. \tag{18}$$

Define a variable $\eta = \omega\tau$. Then, (18) can be expressed as

$$\Delta(\eta) = \mathbf{A} + \mathbf{A}_\tau e^{-j\eta} \tag{19}$$

$e^{-j\eta}$ changes periodically with η, and the period is 2π. Thus, $\Delta(\eta)$ also changes periodically with a 2π period. We can change η within one period $[0, 2\pi]$ and get the root loci of the generalized eigenvalues of $\Delta(\eta)$ within the range $\eta \in [0, 2\pi]$. If there exist eigenvalues $\pm j\omega_c$ on the imaginary axis at η_c, the corresponding critical time delay τ_c can be obtained by $\tau_c = \eta_c/\omega_c$.

Consider a case where communication time delays exist in the studied system with the secondary frequency control gains $K_{p\omega} = 2$, $K_{i\omega} = 60$. In this case, the root loci of $\Delta(\eta)$ within the range $\eta \in [0, 2\pi]$ is shown in Fig. 4. It is shown from Fig. 4 that there are two pairs of general conjugate eigenvalues on the imaginary axis denoted by $\pm j\omega_{d1}$ and $\pm j\omega_{d2}$. Their corresponding critical time delays are denoted by τ_{c1} and τ_{c2}, respectively. The delay margin τ_d is the minimum one between τ_{c1} and τ_{c2}, which is described as $\tau_d = \min\{\tau_{c1}, \tau_{c2}\}$. In this case, $\tau_d = 0.2053$ s.

Therefore, provided there exist L critical time delays denoted by $\tau_{c1}, \tau_{c2}, \ldots, \tau_{cL}$, the delay margin τ_d is $\tau_d = \min\{\tau_{c1}, \tau_{c2}, \ldots, \tau_{cL}\}$. Delay margins with respect to different $K_{p\omega}$ and $K_{i\omega}$ are obtained for the studied system by using the described method above. The results are shown in Fig. 5. It can be found that the delay margin τ_d increases with the increase of the proportional gains $K_{p\omega}$ when $K_{i\omega}$ are fixed, whereas for fixed $K_{p\omega}$, the delay margin τ_d increases with the decrease of the integral gains $K_{i\omega}$.

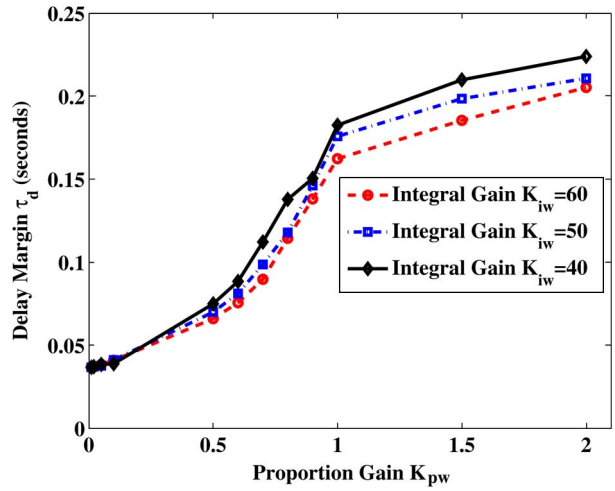

Fig. 5. Relationship between delay margin τ_d and secondary frequency control gains $K_{p\omega}$ and $K_{i\omega}$.

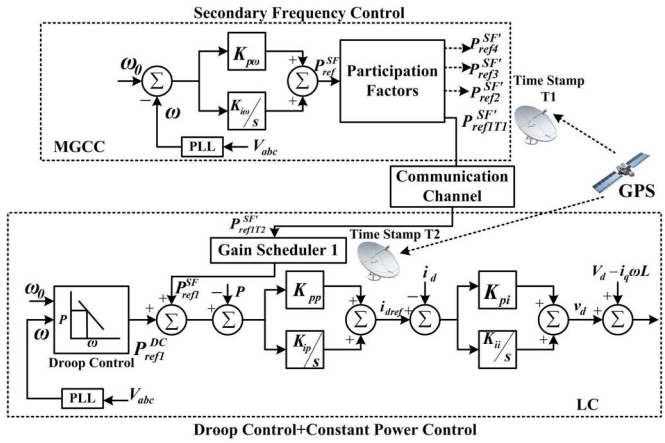

Fig. 6. Control structure of the gain-scheduling approach.

III. Gain-Scheduling Methodology

A. General Control Structure

The presence of communication delays, which are usually time varying in the microgrid frequency control loop, may degrade its performance. A gain-scheduling approach is proposed to compensate the effect of communication delays on the dynamic performance of the islanded microgrid shown in Fig. 1. The microgrid control structure, including both the MGCC and one LC equipped with a gain scheduler, is shown in Fig. 6. Here, we define

$$\bar{K}_{i\omega i} = \beta_{i\omega i} K_{i\omega i} \tag{20}$$
$$\bar{K}_{p\omega i} = \beta_{p\omega i} K_{p\omega i} \tag{21}$$

where $K_{i\omega i}$ and $K_{p\omega i}$ are considered to be fixed since the secondary frequency controller located in the MGCC. The changeable parts are $\beta_{i\omega i}$ or $\beta_{p\omega i}$ located in each local DG controller.

$\beta_{i\omega i}$ denotes an integral gain scheduler denoted and $\beta_{p\omega i}$ denotes a proportional gain scheduler. $\bar{K}_{i\omega i}$ and $\bar{K}_{p\omega i}$ represent the equivalent gains of the secondary frequency controller after gain schedulers are equipped in each LC. We consider that the gain schedulers change only one gain variable, either $\beta_{i\omega i}$ or $\beta_{p\omega i}$. Although simultaneously changing, both of the gain variables can achieve the same purpose; it involves more complicated feasible gain search calculation. The procedure of the gain-scheduling approach includes the following steps.

1) Step 1: The secondary frequency controller in the MGCC calculates real-power set points for each DG to restore their frequencies to the nominal one and sends them to local inverters. These set points are denoted by $P^{\mathrm{SF}'}_{\mathrm{ref}iT_1}$, where T_1 is the time stamp generated when they are sent by the MGCC.
2) Step 2: After LCs in the local inverters receive their set points from the MGCC, the set points are marked as $P^{\mathrm{SF}'}_{\mathrm{ref}iT_2}$, where T_2 is the time stamp generated when they are received by LCs.
3) Step 3: LCs calculate the communication delay by comparing the time stamps of two signals $P^{\mathrm{SF}'}_{\mathrm{ref}iT_2}$ and $P^{\mathrm{SF}'}_{\mathrm{ref}iT_1}$. The time delay is $\tau_i = T_2 - T_1$.
4) Step 4: For a given cost index, by looking up the relationship between the time delay τ_i and its corresponding feasible gain $\beta^{\tau_i}_{i\omega i}$ or $\beta^{\tau_i}_{p\omega i}$ built by the offline analysis, the local gain scheduler adjusts its gain value according to the measured communication delay.

B. Feasible Gain Sets

To find feasible $\beta_{i\omega i}$ and $\beta_{p\omega i}$ that correspond to communication delays, we need to investigate the root locus of the time-delay small-signal model of the microgrid with respect to $\beta_{i\omega i}$ and $\beta_{p\omega i}$.

Considering (20) or (21), the equalized load frequency controller has the following form:

$$P^{\mathrm{SF}}_{\mathrm{ref}i} = \left(K_{p\omega i} + \frac{\bar{K}_{i\omega i}}{s}\right)(\omega_0 - \omega_i) \tag{22}$$

or

$$P^{\mathrm{SF}}_{\mathrm{ref}i} = \left(\bar{K}_{p\omega i} + \frac{K_{i\omega i}}{s}\right)(\omega_0 - \omega_i). \tag{23}$$

The time-delay small-signal model of the microgrid is built as follows:

$$\bar{\mathbf{E}}\Delta\dot{\mathbf{x}} = \bar{\mathbf{A}}\Delta\mathbf{x} + \bar{\mathbf{A}}_\tau\Delta\mathbf{x}(\mathbf{t}-\tau) + \bar{\mathbf{F}}\mathbf{r_0} \tag{24}$$

where $\bar{\mathbf{E}}$ and $\bar{\mathbf{A}}$ are system matrices, $\bar{\mathbf{A}}_\tau$ is a parameter matrix related to the delayed state $\mathbf{x}(\mathbf{t}-\tau)$, and $\bar{\mathbf{F}}$ is a parameter matrix. While most elements of the matrices are still the same as those in (14), the original $K_{i\omega i}$ is replaced by $\bar{K}_{i\omega i}$ or $K_{p\omega i}$ by $\bar{K}_{p\omega i}$. The gain-scheduler vectors $\boldsymbol{\beta}_{\mathbf{i\omega}}$ and $\boldsymbol{\beta}_{\mathbf{p\omega}}$ denote four integral gain schedulers and proportional gain schedulers, respectively.

The characteristic equation of the delayed descriptor system (24) is

$$\det\left(\lambda\bar{\mathbf{E}} - \Delta(\lambda)\right) = 0 \tag{25}$$

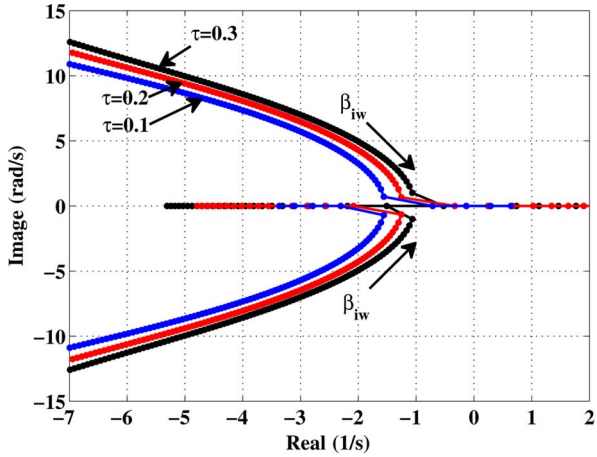

Fig. 7. Root locus for $\boldsymbol{\beta}_{\mathbf{i\omega}}$ under different time delays (arrows direct the increasing gains).

where the characteristic matrix $\Delta(\lambda)$ is

$$\Delta(\lambda) = \bar{\mathbf{A}} + \bar{\mathbf{A}}_\tau e^{-\lambda\tau}. \tag{26}$$

Since the characteristic matrix (26) is transcendent, it has infinitely many roots. Therefore, we can only approximate the solution of (26) by computing a reduced set of its roots. One effective technique is to approximate the roots of (26) by a finite-element method [33]. In this method, matrix $\mathbf{M}$, which has the following form is defined:

$$\mathbf{M} = \begin{bmatrix} & \bar{\mathbf{C}} \otimes \mathbf{I_n} & \\ \mathbf{A}_\tau & \mathbf{0} & \mathbf{A} \end{bmatrix} \tag{27}$$

where $\otimes$ indicate Kronecker's product, $\mathbf{I_n}$ is the identity matrix of order n, and $\bar{\mathbf{C}}$ is a matrix composed of the first $N-1$ rows of $\mathbf{C}$ defined as follows:

$$\mathbf{C} = -2\mathbf{D_N}/\tau \tag{28}$$

where $\mathbf{D_N}$ is a Chebyshev's differentiation matrix of dimension $(N+1)\times(N+1)$ (see Appendix II in [33] for details). Then, the eigenvalues of $\mathbf{M}$ are an approximated spectrum of (26).

For the purpose of demonstrations, N is chosen as 2 for $\mathbf{D_N}$ here. Then, the root locus of the critical eigen pair (which has the smallest damping ratio) of the microgrid system shown in Fig. 1 are investigated for both $\boldsymbol{\beta}_{\mathbf{i\omega}}$ and $\boldsymbol{\beta}_{\mathbf{p\omega}}$ under different time delays $\tau = \{0.1, 0.2, 0.3\}$, as shown in Figs. 7 and 8. From these two figures, it can be seen that feasible gain sets that guarantee the microgrid system stable for both $\boldsymbol{\beta}_{\mathbf{i\omega}}$ and $\boldsymbol{\beta}_{\mathbf{p\omega}}$ become smaller as time delays increase in communication links.

C. Relationships Between Gain-Scheduler Variables and Costs

To find relationships between the gain-scheduler variables ($\beta_{i\omega i}$ and $\beta_{p\omega i}$) and the system performance of the microgrid, the following average squared error is defined as the cost function:

$$J = \frac{1}{T}\int_{t=0}^{T} e_i^2(t) \tag{29}$$

where T is the simulation horizon, and $e_i(t) = \omega_i^d(t) - \omega_i^0(t)$ is the frequency error with respect to the nominal frequency

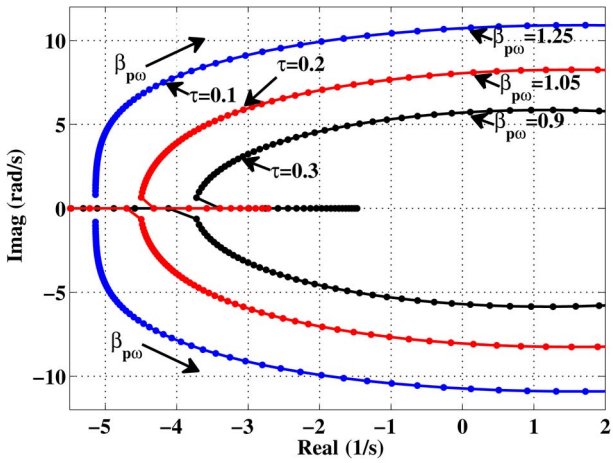

Fig. 8. Root locus for $\beta_{p\omega}$ under different time delays (arrows direct the increasing gains).

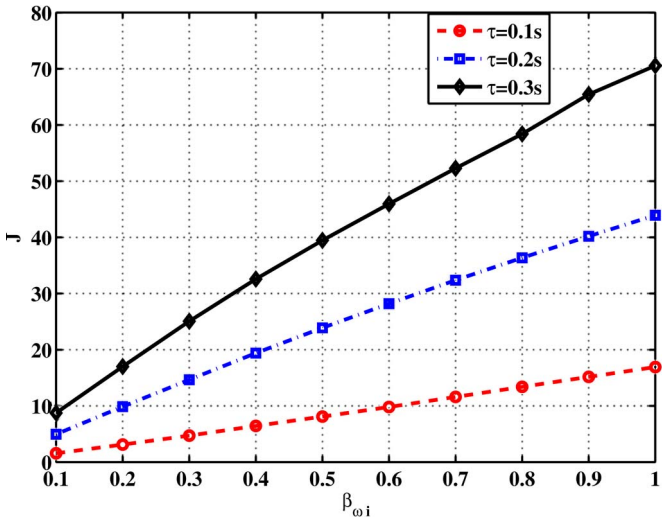

Fig. 9. Cost curve with respect to $\beta_{i\omega 1}$ when $K_{p\omega} = 2$.

reference $\omega_i^0(t)$ for DG i. The nominal reference $\omega_i^0(t)$ is the frequency dynamic of the original DG i when the microgrid operates without communication delays with initial gains $K_{i\omega} = 60$ and $K_{p\omega} = 2$, whereas $\omega_i^d(t)$ is the frequency dynamic of the original DG i when the microgrid runs with communication delays.

Time-domain simulation trials of the microgrid in MATLAB/SimPower R2007b are carried out and the simulations last $T = 3$ s. The $\beta_{i\omega i}$ and $\beta_{p\omega i}$ are investigated, respectively. The performance cost curves with respect to $\beta_{i\omega 1}$ and $\beta_{p\omega 1}$ for DG 1 are shown in Figs. 9 and 10, respectively. From these two figures, it can be seen that the relationship between the cost J and the gain parameter (β_{iw1} or β_{pw1}.) is nearly linear. By the comparison of the results shown in these figures, we can notice that the cost is more sensitive to β_{iw1} than β_{pw1}. Therefore, the dynamic performance of the microgrid is more sensitive to β_{iw1} when time delays are considered.

IV. Validation Studies

The Canadian urban distribution system shown in Fig. 1 is used to study the effect of communication delays on the dynamic performance of an islanded microgrid with a secondary

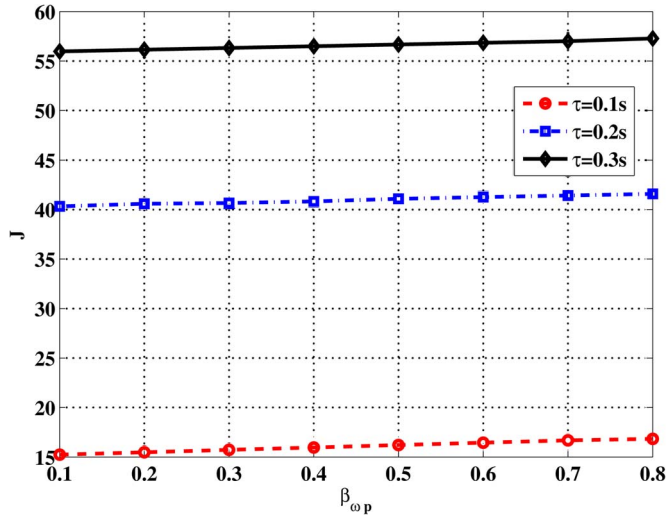

Fig. 10. Cost curve with respect to $\beta_{p\omega 1}$ when $K_{i\omega} = 60$.

frequency controller. In addition, the calculated delay margins and the effectiveness of the proposed gain-scheduling approach are verified. The CB at 120 kV and the 12.5 kV substation is considered to be open at $t = 0.5$ s that means the microgrid is islanded at $t = 0.5$ s. As indicated in the Table II, the coupling filter inductance $L_s = 1$ mH. This is reasonable for the 2 MVA DG. In practice, both $L_s = 1.0$ mH and $L_s = 2.1$ mH have been used for microgrids in [8] and [34]. By implementing a smaller inductance, the stability of the microgrid could be enhanced. The nominal frequency is chosen as $\omega_0 = 377$ rad/s (60 Hz) for the secondary frequency control. This nominal frequency is identical to the current Northern American standard frequency, which guarantees the easy reconnection of the microgrid to the utility main grid.

The small-signal model of this microgrid with 4 DGs is represented by its average inverter model (Simulink Average Model) in MATLAB/SimPower environment. This model has also been verified by comparing with simulations in PSCAD/EMTDC in our previous work [16], [35]. Its secondary frequency controller gains are initially set to $K_{p\omega} = 2$ and $K_{i\omega} = 60$ based on results of the small-signal analysis of the microgrid.

First, the following two cases are tested to evaluate the robustness of the secondary frequency control in the microgrid to loads that have plug and play feature.

1) Case 1: A 0.5-MVA load in the first DG area is plugged in the microgrid at $t = 3$ s.
2) Case 2: A 0.5-MVA load in the first DG area is removed from the microgrid at $t = 3$ s.

The results of these two cases are shown in Figs. 11 and 12. It can be seen the microgrid dynamic is kept stable when a 0.5-MVA load is either plugged in or removed from the microgrid. Therefore, the secondary frequency control can improve the robustness of the microgrid to load changes after being islanded from the main grid by changing the power generation reference.

Then, in order to illustrate the effect of communication delays and verify the calculated delay margin, the following four cases are investigated.

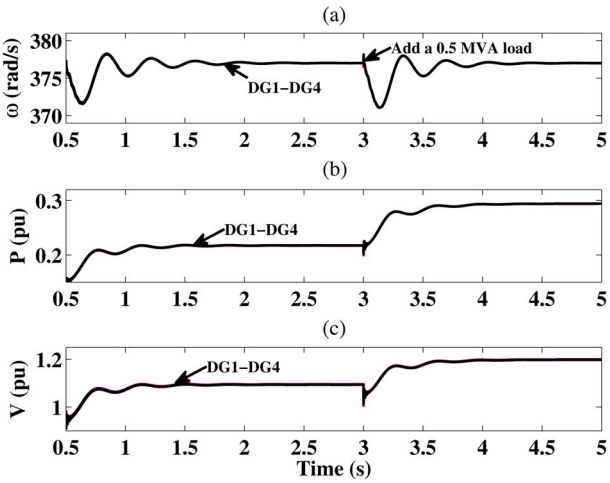

Fig. 11. Dynamic performance of the microgrid when a 0.5-MVA load is added.

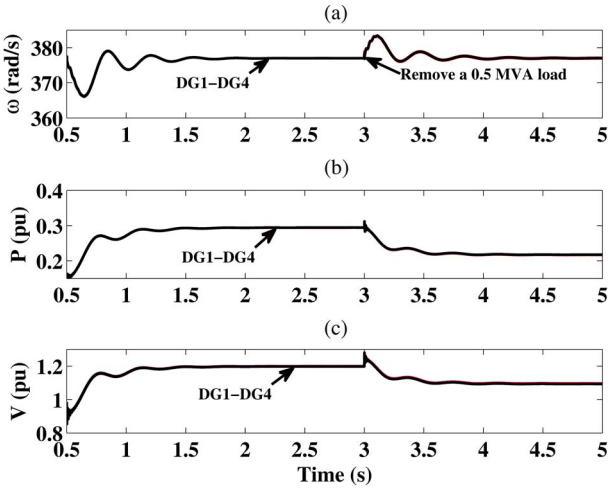

Fig. 12. Dynamic performance of the microgrid when a 0.5-MVA load is removed.

1) Case 3: there is no communication delay in the microgrid.
2) Case 4: there is a constant total communication delay $\tau = 0.1$ s in the microgrid.
3) Case 5: there is a constant total communication delay $\tau = 0.15$ s in the microgrid.
4) Case 6: there is a constant total communication delay $\tau = 0.22$ s in the microgrid.

The results for these four cases are shown from Figs. 13–16, respectively.

When there is no communication delay in the microgrid, it can be seen that the frequency dynamic of the microgrid with four identical DGs oscillates due to the islanding action and then converges fast (at 1.5–2 s) to the nominal frequency 377 rad/s with the hierarchical inverter controllers, as shown in Fig. 13. This observation verifies the theoretical results we just obtained above.

When the time delay increases to $\tau = 0.1$ s and $\tau = 0.15$ s, the magnitude of the frequency oscillation greatly increases after the islanding action is taken, as shown in Figs. 14 and 15. It is noted that time delays could increase the original frequency oscillation resulting from islanding actions.

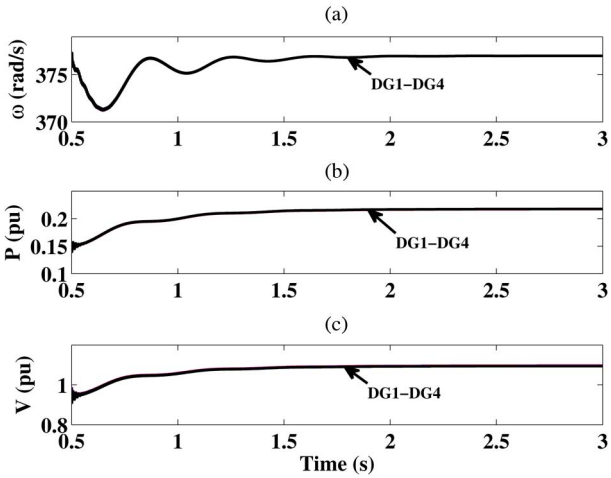

Fig. 13. Dynamic performance of the microgrid when $\tau = 0$ s.

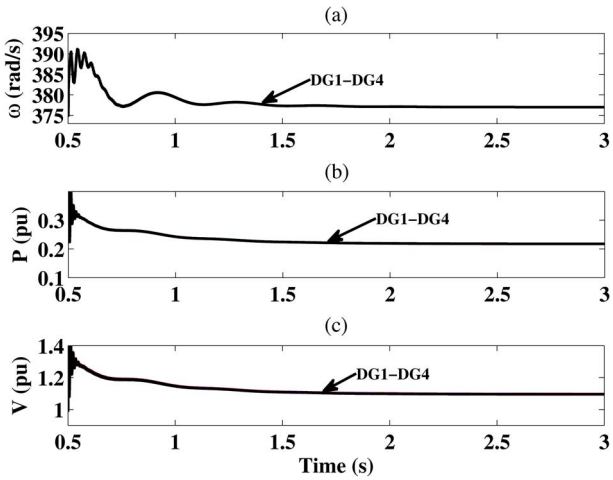

Fig. 14. Dynamic performance of the microgrid when $\tau = 0.1$ s.

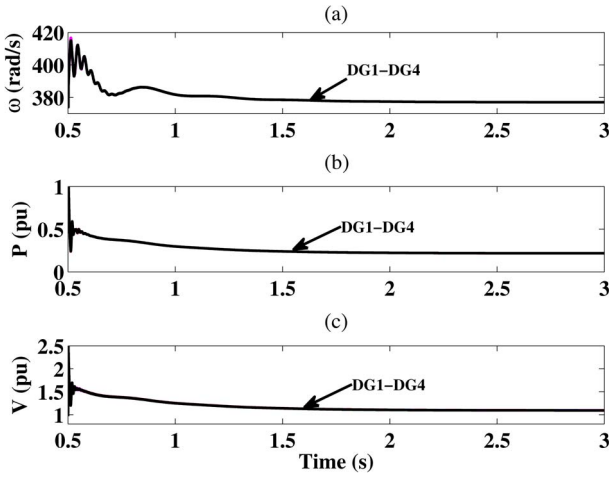

Fig. 15. Dynamic performance of the microgrid when $\tau = 0.15$ s.

When we continue increasing the time delay to $\tau = 0.22$ s, the dynamic performances of the microgrid become unstable, as shown in Fig. 16. It can be noticed that the calculated delay margin for $K_{p\omega} = 2$ and $K_{i\omega} = 60$ is $\tau_d = 0.2053$ s, as shown in Fig. 4. This calculated delay margin closely coincides with the delay margin estimated by the time-domain simulation.

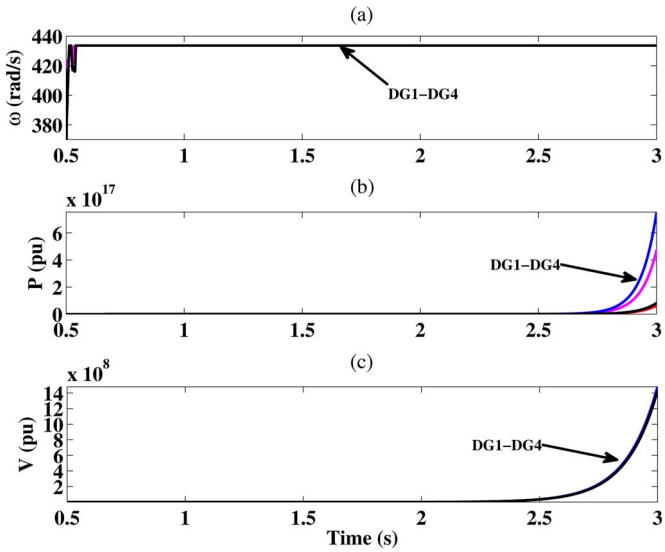

Fig. 16. Dynamic performance of the microgrid when $\tau = 0.22$ s.

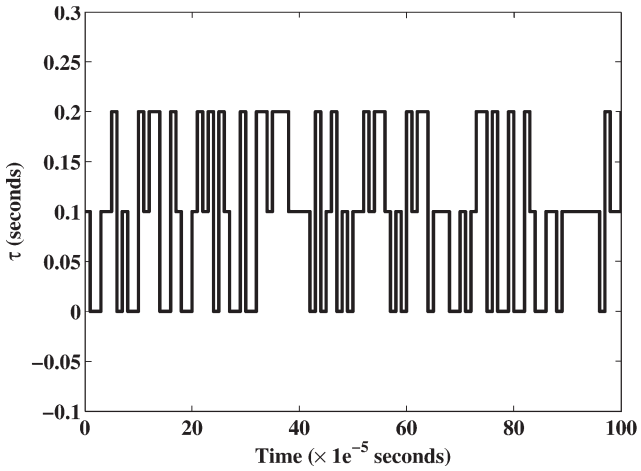

Fig. 17. Dynamic of the time-varying delay (only showing first 100 samples).

Therefore, the presented delay margin calculation method also works well.

Moreover, to evaluate the proposed gain-scheduling approach, the following cases are considered.

1) Case 7: there is a time-varying delay following a uniform distribution with $\tau \in \{0, 0.1, 0.2\}$ with $\beta_{i\omega i}$ gain schedulers in the microgrid.
2) Case 8: there is a time-varying delay following a uniform distribution with $\tau \in \{0, 0.1, 0.2\}$ with $\beta_{p\omega i}$ gain schedulers in the microgrid.

A part of the time-varying delay dynamic is shown in Fig. 17. This time-varying delay follows a uniform distribution, in which the delay varies within {0, 0.1, 0.2} with the same probability. Simulation results of these two cases (only DG1) are shown in Figs. 18 and 19. The microgrid performances with gain schedulers are compared with those without gain schedulers. The frequency oscillation in the microgrid with either integral or proportional gain schedulers is better damped with comparison to the case that no gain scheduler is implemented. The effectiveness of the gain scheduling approach is therefore validated.

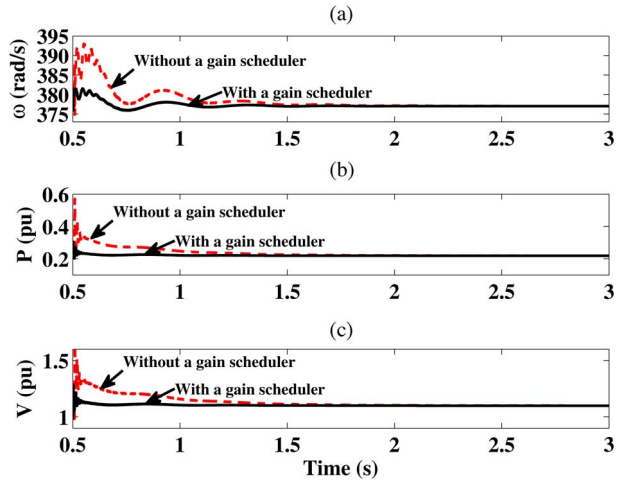

Fig. 18. Dynamic performances of DG1 with a $\beta_{i\omega 1}$ gain scheduler.

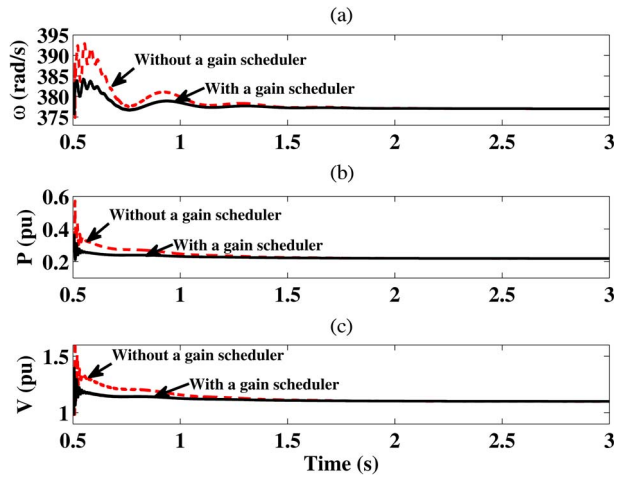

Fig. 19. Dynamic performances of DG1 with a $\beta_{p\omega 1}$ gain scheduler.

V. Discussions on the Hierarchical Frequency Control of Inverter-Based Microgrids

In traditional bulk power systems, the frequency regulation has a hierarchical structure that includes a primary control and a secondary control. In the primary control, a local turbine governor of each generation unit responds to small and fast disturbances such as small load changes, whereas the secondary control utilizes automatic generation control to remove the steady-state frequency error to the nominal value resulted from large disturbances such as islanding actions and short-circuit faults of the grid. In traditional power systems, generation units usually have large inertias, and their responses to the frequency control are slow. Typically, the primary control time is smaller than 10 s, and the secondary control time is between 10 s and 3 min. Being different from traditional power systems, inverter-based distributed generators (DGs) in microgrids can act very fast to load changes and disturbances because of their negligible inertias. Therefore, after receiving the supplementary set points generated by the secondary controller in the MGCC, these DGs can take action in a short time. For example, in [8], the secondary control used only 2.5 s to restore the frequency. In our work, the studied microgrid acts even faster. It can be seen

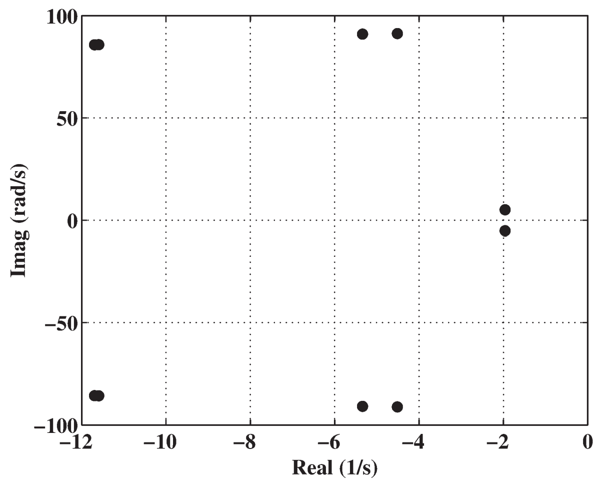

Fig. 20. Plot of eigenvalues of the microgrid system with $K_{p\omega} = 2$ and $K_{i\omega} = 60$.

from the simulation result shown in Fig. 13 that the dynamics of the microgrid system need only about 1.5–2 s. Theoretically, by analyzing the eigenvalues of the microgrid system shown in Fig. 20, it is noted that the absolute value of the real part of the closest conjugate eigenvalues is $\sigma = 2$. According to [36], the settling time of this microgrid system dynamics is around 1.5–2 $((3/\sigma)–(4/\sigma))$ s. This observation coincides with the simulation result. The presence of communication delays when secondary control outputs are transmitted will increase oscillations of the frequency. The gain schedulers in local inverter controllers can be used to better damp these oscillations.

VI. Conclusion and Future Work

This paper has studied the problem how communication delays can affect the secondary frequency control of an islanded microgrid with multiple inverter-based DGs. To investigate this problem, a small-signal model-based method has been introduced to determine the delay margin below which the microgrid maintains stable. By conducting an extensive investigation of different secondary frequency control gains, it has been found that the delay margin increases with the increase of the proportional gains of the secondary frequency controller, whereas it decreases with the increase of the integral gains. To counteract the communication delay effect, a gain scheduling approach has also been proposed for the microgrid secondary frequency control. Results from the Canadian urban distribution system have illustrated the adverse impact of communication delays on the microgrid secondary frequency control and the effectiveness of the proposed gain scheduling approach for compensating the communication delays.

In this paper, the Canadian urban benchmark distribution system is investigated to make the analysis closely related to the practical situation. When the microgrid structure changes, the small-signal model of the microgrid changes and the feasible gain set of the proposed gain scheduling method also changes. The number of total DGs in microgrids and the capacity of each DG also influence the stability of these microgrids. Although the designed gain values to maintain a microgrid stable will be sensitive to the structure of the microgrid, the proposed gain scheduling approach will still be valid since the microgrid can always be modeled in the same way described in this paper (small-signal model), such as [16], [24]–[26], no matter how the structure of the microgrid changes.

In our current work, we mainly focus on the impact of communication delays on the microgrid with inverter-based DGs. However, the effect of communication delays on the microgrid with synchronous machines might not be quite significant, since the reaction speed of synchronous machines is not as fast as the inverter-based DGs. This deserves further investigations and verifications in our future work. In addition, only RLC loads are considered in this work. Nonlinear loads, which can have more complicated impacts on the microgrid, will also be included in future. Last but not the least, a randomly time-varying delay will be modeled and its impact on the microgrid will be deeply investigated in our future work.

Appendix A
Parameter Matrix for the Small-Signal Model

Matrix $\mathbf{E}$ is shown as follows:

$$\mathbf{E} = \begin{bmatrix} \mathbf{E}^{11}_{9\times9} & \mathbf{E}^{12}_{9\times8} \\ \mathbf{E}^{21}_{8\times9} & \mathbf{E}^{22}_{8\times8} \end{bmatrix} \tag{30}$$

$$\mathbf{E}^{11}_{9\times9} = \begin{bmatrix} \mathbf{I} & 0 & 0 & 0 & 0 & 0 & 0 & 0 & 0 \\ 0 & \mathbf{I} & 0 & 0 & 0 & 0 & 0 & 0 & 0 \\ 0 & 0 & \mathbf{L_s} & 0 & 0 & 0 & 0 & 0 & 0 \\ 0 & 0 & 0 & \mathbf{L_s} & 0 & 0 & 0 & 0 & 0 \\ 0 & 0 & \mathbf{k_{pv}} & 0 & -\mathbf{k_{pv}} & 0 & \mathbf{I} & 0 & 0 \\ 0 & 0 & 0 & \mathbf{k_{pv}} & 0 & -\mathbf{k_{pv}} & 0 & \mathbf{I} & 0 \\ 0 & 0 & 0 & 0 & \mathbf{I} & 0 & 0 & 0 & \mathbf{k_{pi}} \\ 0 & 0 & 0 & 0 & 0 & \mathbf{I} & 0 & 0 & 0 \\ 0 & \mathbf{k_{p\omega}} & 0 & 0 & 0 & 0 & 0 & 0 & 0 \end{bmatrix} \tag{31}$$

$$\mathbf{E}^{12}_{9\times8} = \begin{bmatrix} 0 & 0 & 0 & \mathbf{k_{pPLL}} & 0 & 0 & 0 & 0 \\ 0 & 0 & 0 & 0 & 0 & 0 & 0 & 0 \\ 0 & 0 & 0 & 0 & 0 & 0 & 0 & 0 \\ 0 & 0 & 0 & 0 & 0 & 0 & 0 & 0 \\ 0 & 0 & 0 & 0 & 0 & 0 & 0 & 0 \\ 0 & 0 & 0 & 0 & 0 & 0 & 0 & 0 \\ 0 & 0 & 0 & 0 & \mathbf{I} & 0 & 0 & 0 \\ 0 & 0 & 0 & 0 & 0 & 0 & 0 & 0 \\ 0 & \mathbf{I} & 0 & 0 & 0 & 0 & 0 & 0 \end{bmatrix} \tag{32}$$

$$\mathbf{E}^{21}_{8\times9} = [\mathbf{0}]_{8\times9} \tag{33}$$

$$\mathbf{E}^{22}_{8\times8} = [\mathbf{0}]_{8\times8}. \tag{34}$$

Matrix $\mathbf{A}$ is shown as follows:

$$\mathbf{A} = \begin{bmatrix} \mathbf{A}^{11}_{9\times9} & \mathbf{A}^{12}_{9\times8} \\ \mathbf{A}^{21}_{8\times9} & \mathbf{A}^{22}_{8\times8} \end{bmatrix} \tag{35}$$

$$\mathbf{A}^{11}_{9\times9} = \begin{bmatrix} 0 & \mathbf{I} & 0 & 0 & 0 & 0 & 0 & 0 & 0 \\ 0 & 0 & 0 & 0 & 0 & 0 & 0 & 0 & 0 \\ 0 & 0 & 0 & 0 & 0 & 0 & \mathbf{I} & 0 & 0 \\ 0 & 0 & 0 & 0 & 0 & 0 & 0 & \mathbf{I} & 0 \\ 0 & 0 & -\mathbf{k_{iv}} & 0 & \mathbf{k_{iv}} & 0 & 0 & 0 & 0 \\ 0 & 0 & 0 & -\mathbf{k_{iv}} & 0 & \mathbf{k_{iv}} & 0 & 0 & 0 \\ 0 & 0 & 0 & 0 & \mathbf{I} & 0 & 0 & 0 & \mathbf{k_{ii}} \\ 0 & 0 & 0 & 0 & 0 & \mathbf{I} & 0 & 0 & 0 \\ 0 & -\mathbf{k_{i\omega}} & 0 & 0 & 0 & 0 & 0 & 0 & 0 \end{bmatrix} \tag{36}$$

$$\mathbf{A}^{\mathbf{12}}_{\mathbf{9\times 8}}=\begin{bmatrix} 0 & 0 & 0 & k_{iPLL} & 0 & 0 & 0 & 0\\ 0 & 0 & 0 & 0 & 0 & 0 & 0 & 0\\ 0 & 0 & 0 & 0 & 0 & 0 & 0 & 0\\ 0 & 0 & 0 & 0 & 0 & 0 & 0 & 0\\ 0 & 0 & 0 & 0 & 0 & 0 & 0 & 0\\ 0 & 0 & 0 & 0 & 0 & 0 & 0 & 0\\ 0 & k_{pi} & 0 & 0 & 0 & 0 & 0 & 0\\ -k_{ii} & 0 & 0 & 0 & 0 & 0 & 0 & 0\\ 0 & 0 & 0 & 0 & 0 & 0 & 0 & 0 \end{bmatrix} \tag{37}$$

$$\mathbf{A}^{\mathbf{21}}_{\mathbf{8\times 9}}=\begin{bmatrix} 0 & 0 & V_{d0} & V_{q0} & 0 & 0 & 0 & 0 & -I\\ 0 & 0 & -V_{q0} & V_{d0} & 0 & 0 & 0 & 0 & 0\\ aa & 0 & 0 & 0 & 0 & 0 & 0 & 0 & 0\\ bb & 0 & 0 & 0 & 0 & 0 & 0 & 0 & 0\\ cc & 0 & -I & 0 & 0 & 0 & 0 & 0 & 0\\ dd & 0 & 0 & -I & 0 & 0 & 0 & 0 & 0\\ 0 & 0 & 0 & 0 & 0 & 0 & 0 & 0 & 0\\ 0 & 0 & 0 & 0 & 0 & 0 & 0 & 0 & 0 \end{bmatrix} \tag{38}$$

$$\mathbf{A}^{\mathbf{22}}_{\mathbf{8\times 8}}=\begin{bmatrix} 0 & 0 & i_{d0} & i_{q0} & 0 & 0 & 0 & 0\\ -I & 0 & i_{q0} & -i_{q0} & 0 & 0 & 0 & 0\\ 0 & 0 & -I & 0 & 0 & 0 & c0 & s0\\ 0 & 0 & 0 & -I & 0 & 0 & -s0 & c0\\ 0 & 0 & 0 & 0 & c0 & s0 & 0 & 0\\ 0 & 0 & 0 & 0 & -s0 & c0 & 0 & 0\\ 0 & 0 & 0 & 0 & -I & 0 & G & B\\ 0 & 0 & 0 & 0 & 0 & -I & B & G \end{bmatrix}. \tag{39}$$

APPENDIX B
PARAMETERS OF THE STUDIED MICROGRID

TABLE I
DISTRIBUTION SYSTEM PARAMETERS

Parameters	Value
S_{base}	10 (MVA)
V_{base1}	$120\sqrt{2}/\sqrt{3}$ (kV)
V_{base2}	$12.5\sqrt{2}/\sqrt{3}$ (kV)
V_{base3}	$208\sqrt{2}/\sqrt{3}$ (V)
R_S	0 (p.u.)
X_S	0 (p.u.)
R_T	0 (p.u.)
X_T	0.1 (p.u.)
R_f	0.0029 (p.u.)
X_f	0.0041 (p.u.)
R_t	0 (p.u.)
X_t	0.2 (p.u.)

TABLE II
INVERTER PARAMETERS

Parameters	Value
K_{pPLLi}	50
K_{iPLLi}	500
K_{pii}	2.5
K_{iii}	500
L_S	1 (mH)
K_{ppi}	2.5
K_{ipi}	100
$K_{\omega i}$	0.00016
ω_0	377 (rad/s)
$Q_{ref1}, Q_{ref2}, Q_{ref3}, Q_{ref4}$	0 (p.u.)

REFERENCES

[1] R. Lasseter and P. Paigi, "Microgrid: A conceptual solution," in *Proc. 35th IEEE PESC*, 2004, vol. 6, pp. 4285–4290.
[2] R. Lasseter, "Smart distribution: Coupled microgrids," *Proc. IEEE*, vol. 99, no. 6, pp. 1074–1082, Jun. 2011.
[3] H. Farhangi, "The path of the smart grid," *IEEE Power Energy Mag.*, vol. 8, no. 1, pp. 18–28, Jan./Feb. 2010.
[4] F. Katiraei, M. R. Iravani, and P. W. Lehn, "Micro-grid autonomous operation during and subsequent to islanding process," *IEEE Trans. Power Del.*, vol. 20, no. 1, pp. 248–257, Jan. 2005.
[5] M. Chandorkar, D. Divan, and R. Adapa, "Control of parallel connected inverters in standalone AC supply systems," *IEEE Trans. Ind. Appl.*, vol. 29, no. 1, pp. 136–143, Jan./Feb. 1993.
[6] C. Sao and P. Lehn, "Autonomous load sharing of voltage source converters," *IEEE Trans. Power Del.*, vol. 20, no. 2, pp. 1009–1016, Apr. 2005.
[7] J. Guerrero, J. Vasquez, J. Matas, M. Castilla, and L. de Vicuna, "Control strategy for flexible microgrid based on parallel line-interactive ups systems," *IEEE Trans. Ind. Electron.*, vol. 56, no. 3, pp. 726–736, Mar. 2009.
[8] J. Guerrero, J. Vasquez, J. Matas, L. de Vicuna, and M. Castilla, "Hierarchical control of droop-controlled AC and DC microgrids-a general approach toward standardization," *IEEE Trans. Ind. Electron.*, vol. 58, no. 1, pp. 158–172, Jan. 2011.
[9] J. Guerrero, M. Chandorkar, T. Lee, and P. Loh, "Advanced control architectures for intelligent microgrids—Part I: Decentralized and hierarchical control," *IEEE Trans. Ind. Electron.*, vol. 60, no. 4, pp. 1254–1262, Apr. 2013.
[10] J. P. Lopes, C. Moreira, and A. Madureira, "Defining control strategies for microgrids islanded operation," *IEEE Trans. Power Syst.*, vol. 21, no. 2, pp. 916–924, May 2006.
[11] A. Madureira, C. Moreira, and J. P. Lopes, "Secondary load-frequency control for microgrids in islanded operation," in *Proc. Int. Conf. Renew. Energy Power Qual.*, Granada, Spain, 2005, pp. 1–5.
[12] A. Tsikalakis and N. Hatziargyriou, "Centralized control for optimizing microgrids operation," *IEEE Trans. Energy Convers.*, vol. 23, no. 1, pp. 241–248, Mar. 2008.
[13] T. Vandoorn, J. D. M. De Kooning, B. Meersman, and L. Vandevelde, "Communication-based secondary control in microgrids with voltage-based droop control," in *Proc. IEEE PET Trans. Distrib. Conf. Expo.*, May 2012, pp. 1–6.
[14] S.-J. Ahn *et al.*, "Power-sharing method of multiple distributed generators considering control modes and configurations of a microgrid," *IEEE Trans. Power Del.*, vol. 25, no. 3, pp. 2007–2016, Jul. 2010.
[15] Z. Miao, A. Domijan, and L. Fan, "Investigation of microgrids with both inverter interfaced and direct AC-connected distributed energy resources," *IEEE Trans. Power Del.*, vol. 26, no. 3, pp. 1634–1642, Jul. 2011.
[16] X. Wang, W. Freitas, V. Dinavahi, and W. Xu, "Investigation of positive feedback anti-islanding control for multiple inverter-based distributed generators," *IEEE Trans. Power Syst.*, vol. 24, no. 2, pp. 785–795, May 2009.
[17] J. He, C. Lu, X. Jin, and P. Li, "Analysis of time delay effects on wide area damping control," in *Proc. IEEE Asia Pac. Conf. Circuits Syst.*, Nov. 2008, pp. 758–761.
[18] Y. Shi, J. Huang, and B. Yu, "Robust tracking control of networked control systems: Application to a networked DC motor," *IEEE Trans. Ind. Electron.*, vol. 60, no. 12, pp. 5864–5874, Dec. 2013.
[19] H. Li, Z. Sun, M.-Y. Chow, and F. Sun, "Gain-scheduling-based state feedback integral control for networked control systems," *IEEE Trans. Ind. Electron.*, vol. 58, no. 6, pp. 2465–2472, Jun. 2011.
[20] S. Mazumder, M. Tahir, and K. Acharya, "Master-slave current-sharing control of a parallel DC-DC converter system over an RF communication 9 interface," *IEEE Trans. Ind. Electron.*, vol. 55, no. 1, pp. 59–66, Jan. 2008.
[21] F. Liu *et al.*, "Networked multirate output feedback control for setpoints compensation and its application to rougher flotation process," *IEEE Trans. Ind. Electron.*, vol. 61, no. 1, pp. 460–468, Jan. 2014.
[22] F.-L. Lian, W. Moyne, and D. Tilbury, "Network design consideration for distributed control systems," *IEEE Trans. Control Syst. Technol.*, vol. 10, no. 2, pp. 297–307, Mar. 2002.
[23] S. Bukowski and S. J. Ranade, "Communication network requirements for the smart grid and a path for an IP based protocol for customer driven microgrids," in *Proc. IEEE Energytech*, May 2012, pp. 1–6.
[24] N. Pogaku, M. Prodanovic, and T. Green, "Modeling, analysis and testing of autonomous operation of an inverter-based microgrid," *IEEE Trans. Power Electron.*, vol. 22, no. 2, pp. 613–625, Mar. 2007.
[25] N. Pogaku, M. Prodanovic, and T. C. Green, "Inverter-based microgrids: Small-signal modelling and testing," in *Proc. 3rd IET Int. Conf. Power Electron. Mach. Drives*, Apr. 2006, pp. 499–504.

[26] Y. Li and Y. W. Li, "Power management of inverter interfaced autonomous microgrid based on virtual frequency-voltage frame," *IEEE Trans. Smart Grid*, vol. 2, no. 1, pp. 30–40, Mar. 2011.
[27] R. Tonkoski, D. Turcotte, and T. H. M. EL-Fouly, "Impact of high PV penetration on voltage profiles in residential neighborhoods," *IEEE Trans. Sustain. Energy*, vol. 3, no. 3, pp. 518–527, Jul. 2012.
[28] E. P. Dick and A. Narang, "Canadian urban benchmark distribution system," Varennes CETC, Varennes, QC, Canada, Varennes 2005-121, 2005.
[29] L. Dai, *Singular Control Systems*, vol. 118. New York, NY, USA: Springer-Verlag, 1989, ser. Lecture Notes in Control and Information Sciences.
[30] M. Hautus and L. M. Silverman, "System structure and singular control," *Linear Algebra Appl.*, vol. 50, pp. 369–402, Apr. 1983.
[31] L. Jiang, W. Yao, Q. Wu, J. Wen, and S. Cheng, "Delay-dependent stability for load frequency control with constant and time-varying delays," *IEEE Trans. Power Syst.*, vol. 27, no. 2, pp. 932–941, May 2012.
[32] H. Jia and X. Yu, "A simple method for power system stability analysis with multiple time delays," in *Proc. IEEE PES Gen. Meet.*, 2008, pp. 1–7.
[33] F. Milano and M. Anghel, "Impact of time delays on power system stability," *IEEE Trans. Circuits Syst. I, Reg. Papers*, vol. 59, no. 4, pp. 889–900, Apr. 2012.
[34] Z. Ye *et al.*, "Study and development of anti-islanding control for grid-connected inverters," Gen. Elect. Global Res. Center, Niskayuna, NY, USA, May 2004.
[35] X. Wang, "Investigation of positive feedback anti-islanding scheme for inverter-based distributed generation," Ph.D. dissertation, Univ. Alberta, Edmonton, AB, Canada, 2008.
[36] K. Ogata, *Modern Control Engineering*, 5th ed. Boca Raton, FL, USA: Prentice-Hall, 2010.

Shichao Liu received the B.Sc. and M.Sc. degrees from Harbin Engineering University, Harbin, China, in 2007 and 2010, respectively, and the Ph.D. degree from Carleton University, Ottawa, ON, Canada, in 2014.

He is currently a Postdoctoral Fellow with Carleton University. His research interests include networked control systems, energy management, and optimization of microgrids.

Xiaoyu Wang (M'08–SM'13) received the B.Sc. and M.Sc. degrees from Tsinghua University, Beijing, China, in 2000 and 2003, respectively, and the Ph.D. degree from the University of Alberta, Edmonton, AB, Canada, in 2008.

He is currently an Assistant Professor with the Department of Electronics, Carleton University, Ottawa, ON, Canada. His research interests include integration of distributed energy resources and power quality.

Peter Xiaoping Liu (M'02–SM'07) received the B.Sc. and M.Sc. degrees from Northern Jiaotong University, Beijing, China, in 1992 and 1995, respectively, and the Ph.D. degree from the University of Alberta, Edmonton, AB, Canada, in 2002.

He is currently a Canada Research Chair Professor with the Department of Systems and Computer Engineering, Carleton University, Ottawa, ON, Canada. His research interest includes interactive networked systems and teleoperation, haptics, micromanipulation, robotics, intelligent systems, context-aware intelligent networks, and their applications to biomedical engineering.